

# Full-Scale Crash Test of an MD-500 Helicopter

Justin Littell  
ATK Space Systems  
NASA Langley Research Center  
12 W. Bush Rd  
Hampton Virginia, 236881  
[Justin.D.Littell@nasa.gov](mailto:Justin.D.Littell@nasa.gov)

## Abstract

A full-scale crash test was successfully conducted in March 2010 of an MD-500 helicopter at NASA Langley Research Center's Landing and Impact Research Facility. The reasons for conducting this test were threefold: 1 – To generate data to be used with finite element computer modeling efforts, 2 – To study the crashworthiness features typically associated with a small representative helicopter, and 3 – To compare aircraft response to data collected from a previously conducted MD-500 crash test, which included an externally deployable energy absorbing (DEA) concept. Instrumentation on the airframe included accelerometers on various structural components of the airframe; and strain gages on keel beams, skid gear and portions of the skin. Three Anthropomorphic Test Devices and a specialized Human Surrogate Torso Model were also onboard to collect occupant loads for evaluation with common injury risk criteria. This paper presents background and results from this crash test conducted without the DEA concept. These results showed accelerations of approximately 30 to 50 g on the airframe at various locations, little energy attenuation through the airframe, and moderate to high probability of occupant injury for a variety of injury criteria.

## Introduction

The Landing and Impact Research (LandIR) Facility at NASA Langley Research Center (LaRC) has a long history of testing aircraft, rotorcraft and spacecraft. It was originally built as the Lunar Landing Research Facility [1], where Apollo astronauts trained to fly in a simulated lunar landing environment. At the end of the Apollo program, it was converted into a full-scale crash test facility for investigating general aviation (GA) aircraft crashworthiness. Since 1974, over 100 tests have been completed on GA aircraft, helicopters, and fuselage subsections. More recently, the facility supports NASA's Constellation Research Program for Orion crew module landing. The LandIR is shown in Figure 1.



Figure 1 - LandIR Facility at NASA LaRC

---

Presented at the American Helicopter Society 67th Annual Forum, Virginia Beach, VA, May 3-5, 2011. Copyright © 2011 by the American Helicopter Society International, Inc. All rights reserved. This is a work of the U.S. Government and is not subject to copyright protection in the U.S.

The 240 ft. high, 400 ft. long steel gantry structure is unique in that it is capable of imparting both horizontal and vertical velocities simultaneously as the impact conditions, along with a variety of impact attitudes to all types of fixed-wing aircraft, spacecraft and rotorcraft vehicles. Thus, more realistic flight path angles can be achieved compared to purely vertical drop tests. Some examples specific to rotorcraft vehicles previously tested

at LandIR include the ACAP, UH-1, CH-47, UH-60, and AH-1 [2]. Figure 2 shows examples of these vehicles.



Figure 2 – Examples of previously tested rotorcraft

Previous tests of rotorcraft have focused on reducing occupant loads through cabin airbag systems and/or inflatable restraint systems (AH-1), load-limiting seats (UH-60) and evaluating the structural response of the airframes. Also, some of the General Aviation data collected from tests conducted at LandIR was used for FAA guidelines for aircraft seat certification [3-5].

The MD-500 helicopter was the most recent aircraft tested at the LandIR facility. Two full-scale crash tests were

conducted on the helicopter as part of a larger test series in which one of the objectives was to validate a novel deployable energy absorbing concept [6-8] on an actual airframe under realistic crash conditions. For a description of the test which included the DEA see reference [9].

A second objective of the test was to give engineers valuable insight into the response of a small helicopter subject to impact loads. A third objective was to provide validation data for a finite element simulation of the MD-500 crash test [10]. The information presented herein discusses the results obtained for this baseline test of the MD-500 without external energy absorbers.

### Test Article Description

The helicopter used for this test was an MD-500 provided by the US Army. It is a derivative of the Hughes OH-6 helicopter, and the military version of the helicopter is the Defender series. The specifications on this helicopter are listed in Table 1.

Table 1 – MD-500 specifications

Parameter	Value
Maximum Speed	156 knots
Range	300 nautical miles
Empty Weight	1550 lbs
Gross T/O Weight	3000 lbs

Modifications were necessary to prepare the MD-500 helicopter for the test. A summary of the major modifications is as follows:

- Damaged aluminum skin near helicopter tie down points and acrylic windshield panels were replaced or repaired.
- Original oleo-pneumatic skid gear struts were replaced with crushable energy absorbing struts. [9]
- Box beams were added to the front and rear bulkheads to serve as LandIR cabling system attachment points used for lifting and releasing.
- Ballast mass, in the form of lead blocks, was placed in locations representing major structural and mechanical components of the aircraft such as engine and transmission, main rotor, tail rotor, doors, and instrument panel.
- Sand bags were placed in the rear sub-floor to represent the fuel ballast.

- New skid gear was installed.
- New front bucket and rear bench seats were installed.

Minor damage on the skin and front subfloor sustained from the previous test was repaired. The minor damage was caused from the belly skin reacting against the DEA crush during impact. Figure 3 illustrates the damage repaired from the previous testing.

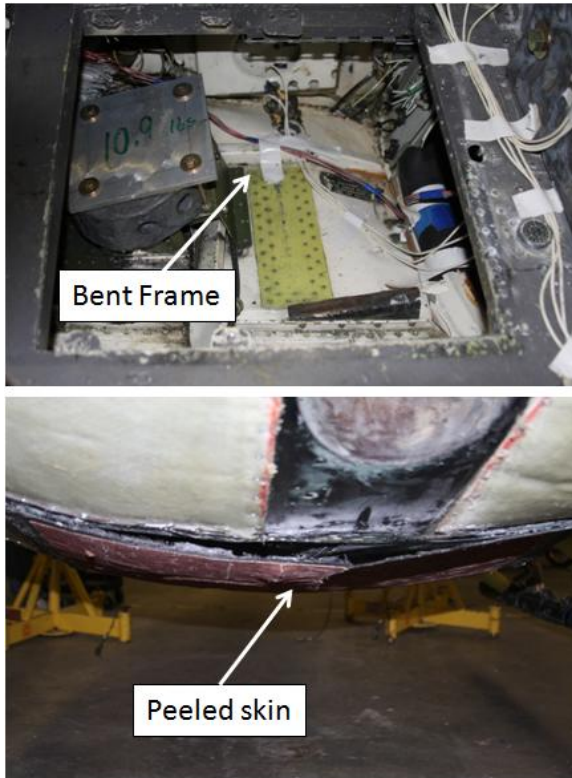


Figure 3 – Damaged areas from first MD-500 test

Figure 3, top, looks into the pilot floor showing the extent of the damage from the previous test. The bent frame was due to the MD-500 belly crushing, shown in figure 3, bottom. Figure 3, bottom, shows damaged belly skin which peeled and separated from the nose. New aluminum sheet metal was fabricated and reinstalled in place of the bent front frame and belly. Note that even though the peeled skin occurred in the nose of the helicopter, the peeling was actually from a doubler material added for the previous test. The doubler material was placed from the nose to the rear bulkhead, and its removal for this test required that parts of the skin also be replaced. Thus skin was replaced for the entire belly. Figure 4 shows the repairs made.

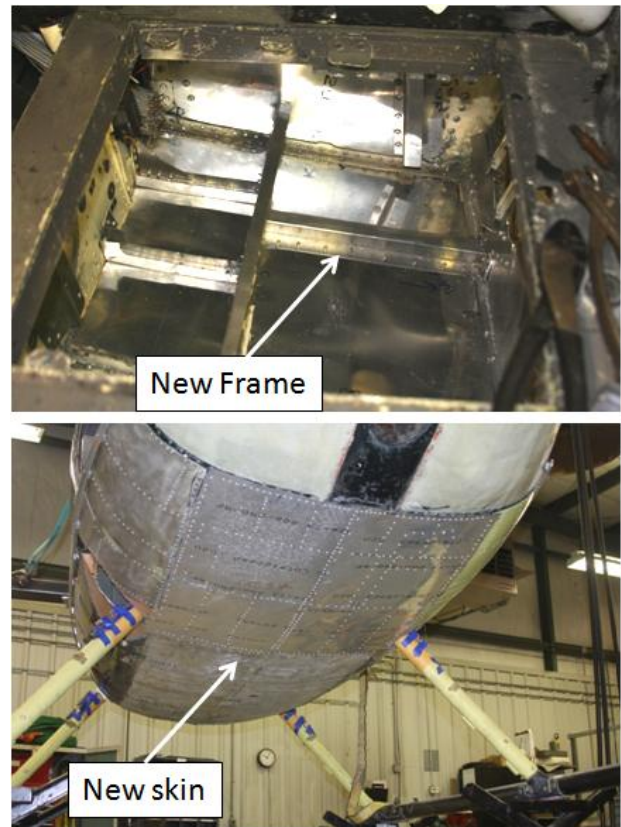


Figure 4 – Repaired regions on MD-500 helicopter

The MD-500 test article weighed 2906 lbs. It was instrumented to collect strain, acceleration, load and Anthropomorphic Test Device (ATD) occupant response data. Accelerometers were located on structural components of the airframe, added ballast locations and floors, while strain gages were placed on the bulkheads, keel beam, and skid gear. Four ATD occupants were placed onboard. The pilot (front left) was a Hybrid III 50<sup>th</sup> percentile ATD containing a FAA approved straight spinal column [11]. The co-pilot (front right) and rear passenger (rear right) were standard Hybrid II 50<sup>th</sup> percentile ATDs. The left rear passenger (rear left) was a specialized human surrogate torso model (HSTM), designed to measure the soft tissue injury on a human torso [12]. The HSTM was an upper body test device only and attached to a standard Hybrid III pelvis. The front pilot and co-pilot were seated in standard mesh cloth bucket seats and restrained with 5-point harnesses. The rear occupants sat on a standard mesh bench seat and restrained with lap and shoulder harnesses only. Figure 5 shows the pre-test configuration of the MD-500 at the LandIR Facility.

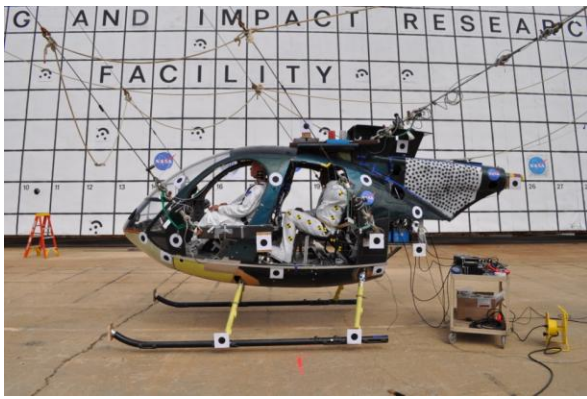


Figure 5 – MD-500 helicopter in test configuration

As mentioned earlier, a previous test at the LandIR facility was completed which evaluated the performance of a DEA structure for the attenuation of impact loads. The test described herein is a replicate of that test; having both the same impact conditions and same helicopter configuration. The helicopter’s impact conditions were nominal 40 ft/sec horizontal and 26 ft/sec vertical velocities giving a resultant velocity of 47.7 ft/sec at a 33 degree glide angle. The impact surface was concrete. The particular velocities were chosen to represent a severe, but survivable crash, though not based on a particular standard such as MIL-STD-1290A [13]. The impact conditions were achieved by swinging the helicopter in a pendulum style using LandIR cabling equipment and hardware through two sets of parallel swing cables, located on either side of the vehicle. After lifting the test article to a required drop height, pyrotechnics severed the pullback cables, allowing the vehicle to swing toward the ground in a pendulum style fashion via the swing cables. Immediately before impact, pyrotechnics severed the swing cables such that free fall conditions were present immediately prior to impact.

## Results

The impact conditions of the airframe, as determined by photogrammetry [14], are listed in Table 2. Linear velocities were determined by averaging all of the rigid body motion of each target on the vehicle immediately before impact. The attitude and angular velocity measurements were taken from angles between a combination of lines and planes on the vehicle and reference planes created computationally in the photogrammetry software.

Table 2 – Impact Conditions

Impact Parameter	Target	Measured
<i>Linear velocity (ft/sec)</i>		
Forward	40.0	39.1
Vertical	26	24.1
Lateral	0	0.6
Resultant	47.7	45.9
<i>Attitude (deg)</i>		
Pitch	0	-6.2
Roll	0	1.9
Yaw	0	2.1
<i>Angular Velocity (deg/sec)</i>		
Pitch Rate	0	0.54
Roll Rate	0	0.68
Yaw Rate	0	1.65

Table 2 shows that both the horizontal and vertical velocities were slightly below the intended nominal conditions. These differences were attributed to air resistance during the pendulum swing. The higher than nominal lateral velocity and roll and yaw attitude are due to the prevailing wind conditions, which pushed the vehicle off-center before and during the swing. A large nose down pitch is present due to the Center of Gravity being slightly forward of the center point of the parallel swing cables. The impact is shown in figure 6, which depicts frames from the high-speed camera in a view normal to the flight path.

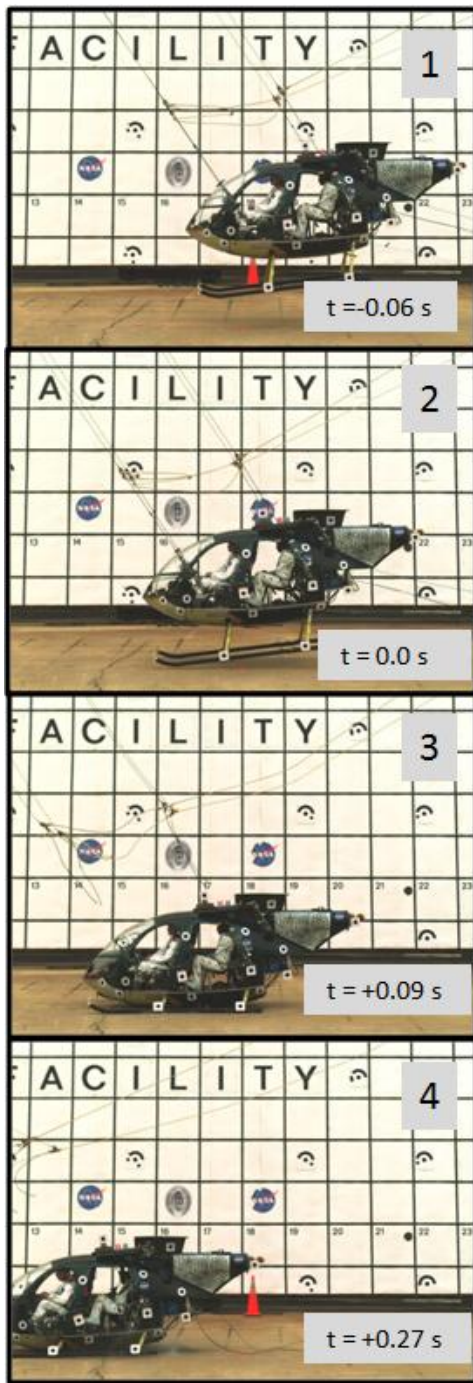


Figure 6 – View from South camera

In figure 6, picture 1 shows the helicopter 0.06 sec before impact. Note that due to the minimal roll and yaw present, the tips of the near skid gear are slightly lower than the tips of the far skid gear. Picture 2 shows the helicopter at the point of first skid gear impact ( $t=0.0$  sec). The far (right) gear impacts the ground first which is due to the minor amount of yaw and roll present. Picture 3 shows the point of maximum vertical displacement, noting the helicopter still has a nose down pitch. Picture

4 shows a post-impact rebound. After the point of maximum vertical deflection, the nose is seen to pitch forward on the rebound, presumably due to the downward pitch of the nose at impact. Figure 7 shows the same four impact times from a camera located on the flight path, in front of the test article.

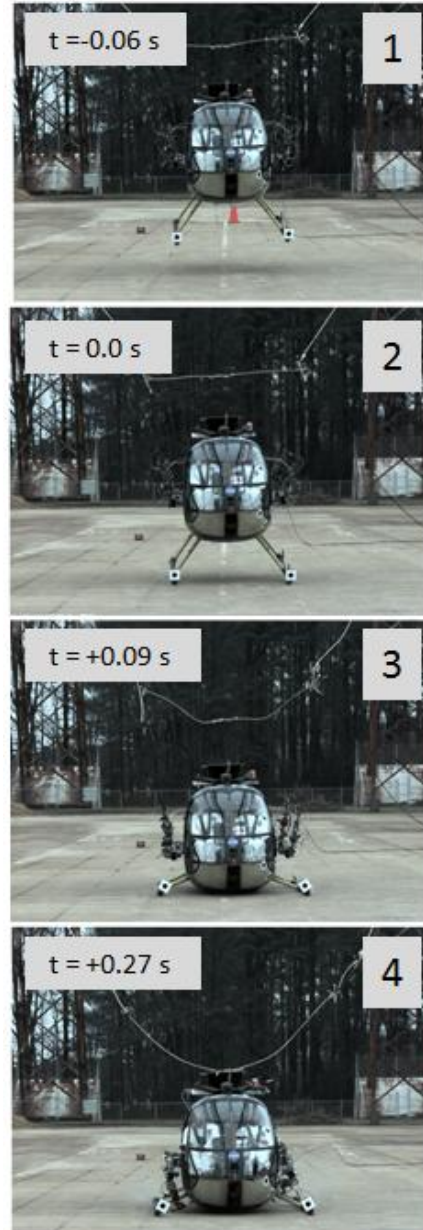


Figure 7 – View from West Camera

Picture 1 in figure 7 shows the MD-500 before impact. Again, the helicopter has a slight yaw, noting the difference between the orange tape on the plexi-glass nose of the test article and the white dotted LandIR centerline extending from the bottom of each picture. Also note the roll present by examining the difference in vertical

position between the left and right skid gear tips. Picture 2 shows skid gear contact with the right gear contacting the ground shortly before the left gear. Picture 3 shows the maximum vertical deflection of the helicopter, while picture 4 shows the helicopter post-impact rebound, where it has pitched down. Ripples in the nose on the pilot side can be seen in pictures 3 and 4, suggesting that parts of the nose structure have failed. Figure 8 shows the MD-500's post test final position.



Figure 8 – Post-impact position of the MD-500 helicopter

Note it has turned slightly to the left, presumably from the amount of yaw present during the impact. The ATD occupants have flailed off to the right. The skid gears are intact suggesting that their energy absorbing features were limited. The helicopter slide-out after impact was 51 ft. 1 in. The test article was examined further after being removed from the impact area. Figures 9 through 11 show some notable airframe damage.



Figure 9 – External skin damage

Figure 9 shows some external skin damage noticed while the MD-500 was being transported away from the impact area. The skin rippling seen on the right side near the right front skid gear attachment is suggestive that the movement of the gear during impact has caused some of

the internal structure on the subfloor to buckle. However, the upper portion of the skin rippling may be artificial due to its proximity to the LandIR front attachment beam. The motion of the attachment beam at impact may have caused the top portion of the rippling. Because no video evidence exists on this specific portion, the exact cause cannot be accurately pinpointed. Following the removal of the MD-500 helicopter post-test, the seats and occupants were removed to examine the floor and subfloor. Figure 10 shows the front subfloor underneath both the pilot and co-pilot.

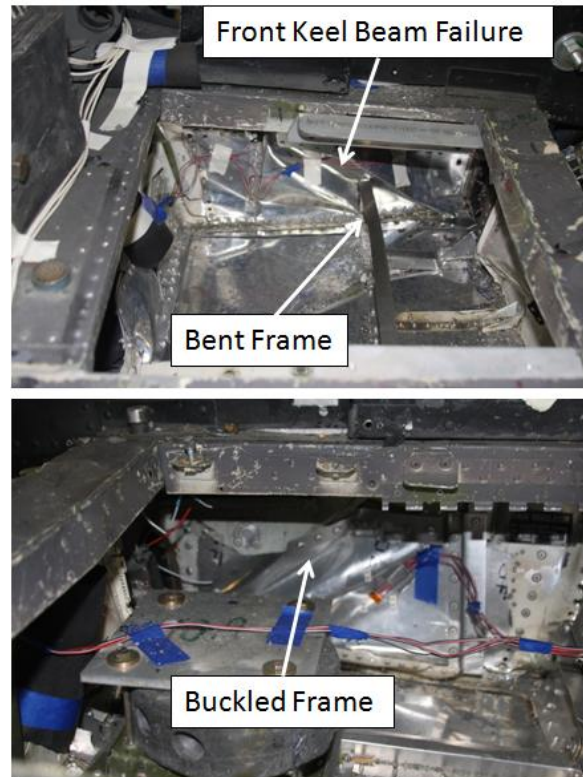


Figure 10 – Co-pilot subfloor (top) and pilot subfloor (bottom)

Much of the subfloor and bottom skin was severely deformed after the test, indicating that these regions absorbed the majority of the impact energy. The center keel beam was severely dented in multiple places from the nose to the rear bulkhead, while the frames extending from the keel beam to the outer structure were bent and buckled in multiple places. Similar damage exists for the pilot side subfloor.

The deformations underneath the rear occupants were next examined.

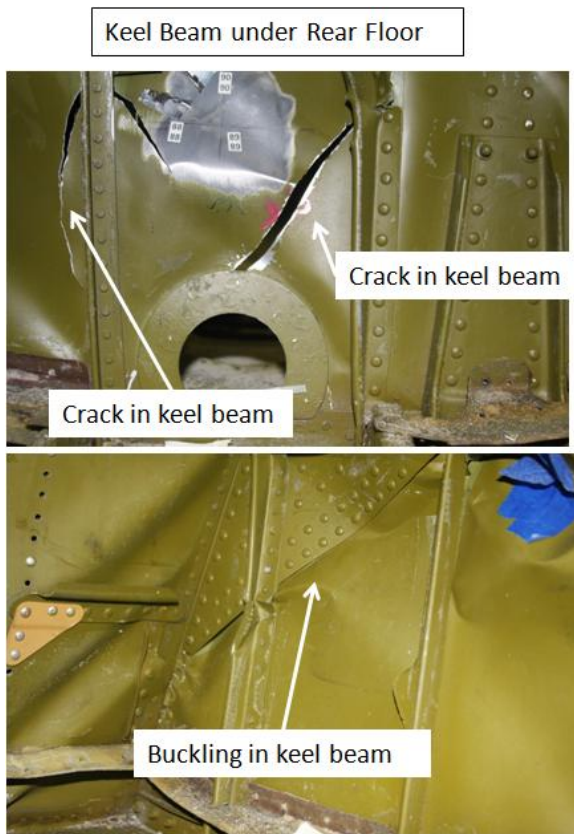


Figure 11 – Rear Floor

Figure 11 shows severe deformations on the keel beam underneath the rear occupants. In many places the beam has buckled and cracked, leaving little to no structural integrity. Much of the upper portion of the airframe was intact post-test suggesting that the loads due to impact were absorbed by deformation and failure of the subfloor structure.

After initial investigations into the visible airframe damage, airframe accelerations were next examined. Figure 12 shows the vertical accelerations compared between the front left and front right floor, underneath the legs of the front occupant, in places near those in figure 10. Acceleration traces were filtered with a 4-pole low-pass Butterworth filter with a cutoff frequency of 60 Hz.

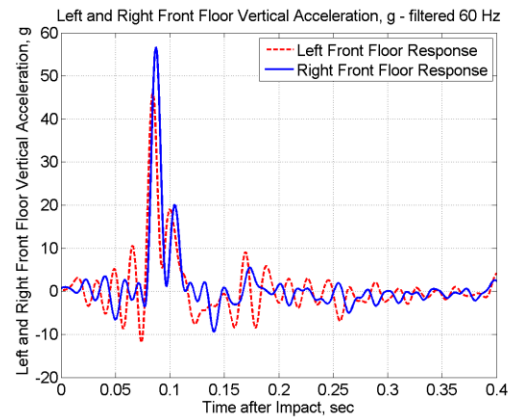


Figure 12 - Left and Right Front Floor Vertical Acceleration

The oscillations seen in figure 12 are oscillations on the floor due to initial skid gear ground contact. Figure 12 shows a distinct large spike at approximately 0.075 sec. after impact, which is attributed to the belly of the airframe impacting the surface. The peak value for the right accelerometer was 56.7 g, while the peak value for the left accelerometer was 45.9 g. The approximate 10 g difference was attributed to the right side impacting the ground first. The second, smaller spike at 0.1 sec is part of the larger initial contact, and is probably due to the inertia of the ATD occupants impacting the seats slightly after the initial belly contact. After the initial spikes, the acceleration traces show no more distinct characteristics.

Figure 13 shows two acceleration traces which contrast the results found in figure 12; one from the rear floor and one from near the top rotor ballast location. Acceleration traces were filtered with a 4-pole low-pass Butterworth filter with a cutoff frequency of 60 Hz.

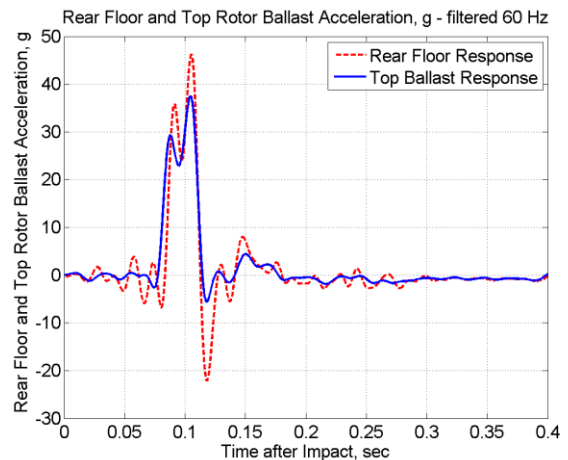


Figure 13 – Rear Floor and Top Ballast Vertical Acceleration

Figure 13 shows two peaks for both the rear floor and the top ballast response locations. Filtering artifacts account for the double peak seen in figure 13, but the shape and relative peak values show that the pulse widths are much longer in the rear and at the top of the helicopter. While the duration of the large front acceleration pulse was approximately 10 ms, the rear and top accelerations were closer to 40 ms. The longer duration was attributed to the subfloor crushing, and thus absorbing much of the initial impact load and lengthening the pulse width. The rear floor showed a higher peak at 46.3 g while the top ballast showed a much lower peak of 37.4 g, demonstrating the dissipation of approximately 10 g by the airframe between the floor and the roof of the cabin.

The acceleration data showed that the airframe experienced an average of 51.3 g for approximately 10 ms in the front of the aircraft and an average of 41.9 g for approximately 40 ms toward the rear. Higher magnitude and shorter duration acceleration data is due to the pitch down attitude, in which the front of the airframe impacted the ground first. The lower magnitude, longer duration accelerations in the rear and on the top of the helicopter suggested that the components in the front and on the floor of the helicopter helped to absorb the impact energy.

Along with examining airframe accelerations, responses of the onboard occupants were examined and injury potential was evaluated using a variety of injury criteria. Figure 14 shows all the pelvis, chest and head accelerations of the pilot, which was a 50<sup>th</sup> percentile Hybrid III ATD. All acceleration traces are unfiltered from post-processing. In all occupant responses, the positive x- axis is oriented from the back to the chest, the positive z- axis is oriented from the pelvis to the head and the right-hand-rule defines the y-axis.

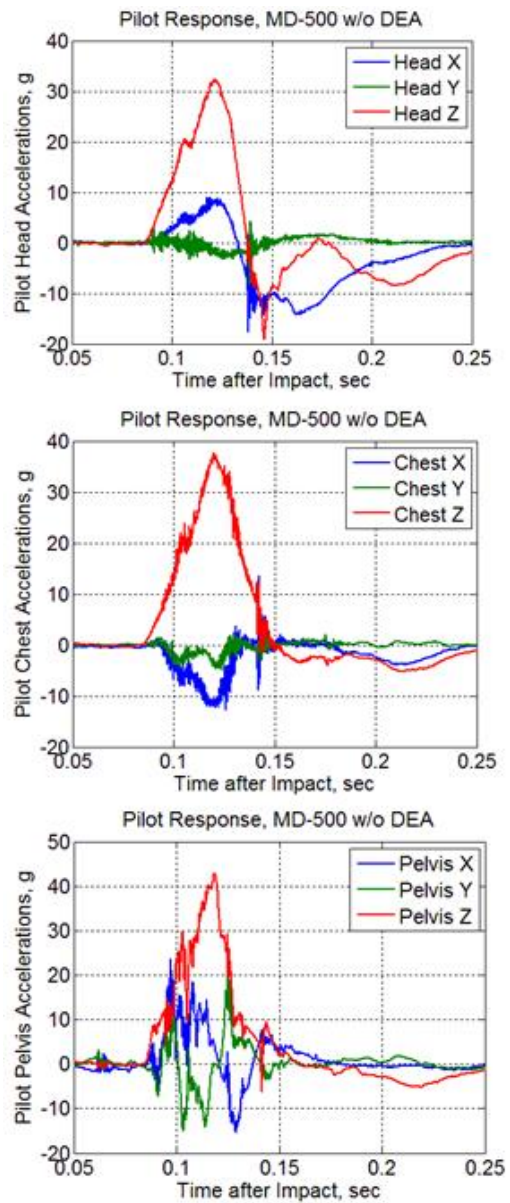


Figure 14 – Pilot accelerations

The pilot head, chest and pelvic accelerations show predictably high magnitudes in the vertical directions, a measureable response in the horizontal direction and a very small response in the lateral direction. These results are expected since the test was conducted primarily in the horizontal and vertical directions only. The peak pelvic, chest, and head vertical accelerations were 42.8 g, 37.8 g and 32.4 g, respectively. The peak pelvic, chest, and head horizontal accelerations were -14.9 g, -12.2 g and -13.9 g, respectively. The decreasing vertical acceleration values seen when going from the pelvis to the head indicates internal attenuation and energy absorbing characteristics from the ATD itself. The horizontal acceleration stayed approximately the same for all three locations, presumably because the restraint systems present. Both

the pilot and co-pilot ATD were restrained in 5-point harnesses tightened as tight as possible, which effectively restricted the dummy motion in the horizontal direction, leading to large, non-decreasing acceleration values.

As with the pilot, the co-pilot head, chest and pelvis accelerations are shown in figure 15. Again, all acceleration traces are unfiltered.

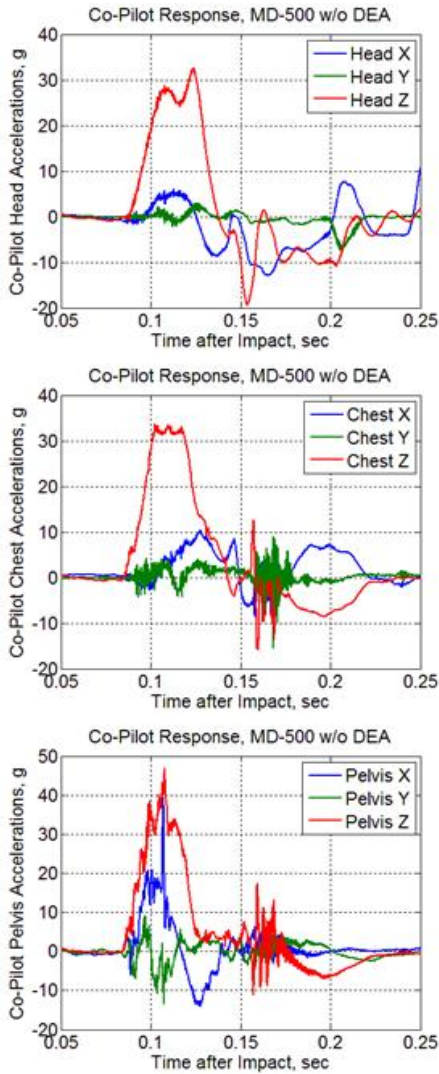


Figure 15 – Co-pilot accelerations

The co-pilot pelvis, chest and head vertical accelerations were 46.6 g, 33.7 g, and 32.6 g, respectively. The co-pilot pelvis, chest and head horizontal accelerations were 20.8 g, 10.2 g, and -12.4 g respectively. The vertical accelerations exhibit the same trend as the pilot accelerations; decreasing as the load goes from the pelvis to the head, indicating internal attenuation. The horizontal accelerations do not exhibit the same trends as the pilot. This finding could possibly be due to a difference in the tightness of the restraint systems, or

possibly because the co-pilot’s side of the helicopter impacted the ground first. In this case, the friction between the skid gear and ground might have caused the horizontal acceleration to be much higher in the co-pilot. It should be noted that the general shape of the curves are very similar, with the exception of a minor plateau for the vertical acceleration. The plateau could be due to a small piece of foam that was placed underneath the co-pilot seat, between the seat mesh and the seat box.

Finally, the rear passenger head, chest and pelvic were examined as shown in figure 16. As with the pilot and co-pilot, all acceleration traces are unfiltered.

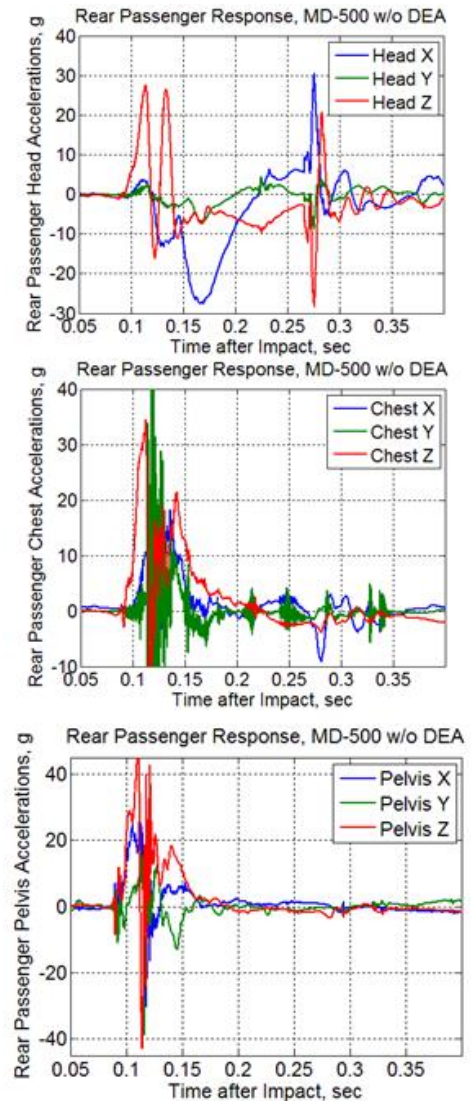


Figure 16 – Rear Passenger accelerations

The rear passenger pelvis, chest and head vertical accelerations were 46.5 g, 34.4 g, and 27.1 g respectively. The rear passenger pelvis, chest and head horizontal accelerations were 25.2 g, 18.2 g, and -26.7 g

respectively. As seen with the other two occupants, generally, the trends matched in the vertical direction. Attenuation between the pelvis and head was seen, however the shape of the vertical acceleration curves was different. This difference was presumably from the fact that the rear ATD was seated on a different (bench) seat. A trend could not be seen in the horizontal accelerations, as the data was scattered between the head, chest and pelvis. One possible reason for this scatter is the restraint system. Instead of having a 5-point harness restraint system which fully constrained the front ATDs, the rear ATD had only a lap and shoulder belt, much like the seatbelts found in automobiles. The lack of reaction force from a full restraint probably attributed to the discrepancies seen.

The acceleration time histories were compared to a series of injury curves originally developed by Eiband [15] in the late 1950s. Eiband summarized the available literature and proposed injury limit curves for humans subject to loads in all three independent axes. In his work, he proposed that injury was dependent on both the duration and magnitude of the peaks of the acceleration. Figure 17 shows an example of one of Eiband’s curves, depicting injury thresholds for accelerations in the vertical direction. It is this curve that will be used as the basis for comparison for the acceleration traces from the test.

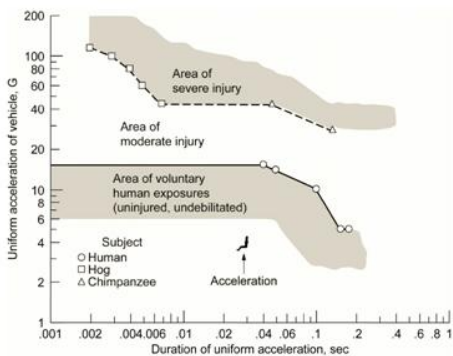


Figure 17 – Injury Limit Curve originally developed by Eiband and reproduced from [19]

Table 3 shows the peak and estimated duration of uniform acceleration for each of the three occupants in the vertical direction, along with the value read from the plot in figure 17. The peaks and duration are taken from the seat pans.

Table 3 – Seat Pan Vertical Acceleration Peaks and Durations

Position	Peak (g)	Duration (sec)	Eiband Regime
Pilot	63.1	0.023	Severe Injury
Co-pilot	53.4	0.024	Severe Injury
Rear Passenger	27.2	0.021	Moderate Injury

A load cell capable of measuring compressive loading in the lumbar region was also present in three of the four onboard occupants. The time histories of these loads are shown in figure 18. Note that a positive value indicates a compressive load.

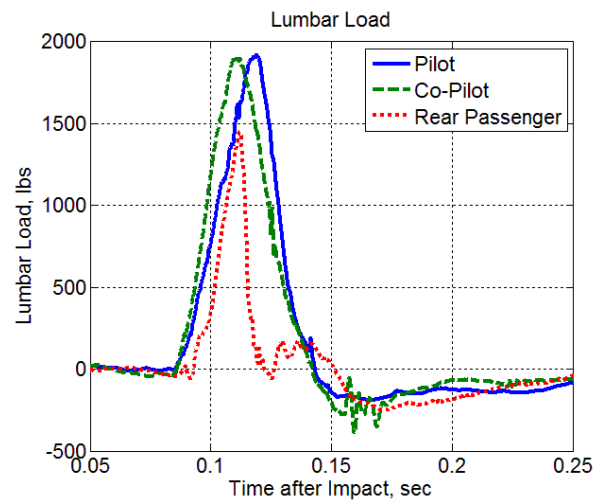


Figure 18 – Occupant Lumbar Loads

The resulting lumbar loads were 1,919, 1,901 and 1,449 lbs for the pilot, co-pilot and rear passenger, respectively. Lumbar loads were filtered at SAE CFC 600, with accordance with SAE J211 [16]. The pilot and co-pilot’s compressive lumbar loads reached similar magnitudes and durations, presumably because they were seated in similar mesh bucket seats. The co-pilot reaches the peak value first, presumably because the helicopter’s right side impacted first. The rear passenger’s time history is slightly different due to its position on a bench seat.

The load values are important because FAR Part 27.562 (c) [3] establishes a lumbar limit of 1,500 lb as being injurious. The loads incurred in the occupants were over the limit for the front occupants and only slightly below it for the rear occupant. The lumbar load results agree with the results seen from the Eiband criteria, suggesting

confidence can be gained from the correlation between the two.

The pilot, co-pilot and rear passenger seat pan accelerations were also input into the Brinkley model [17], which is used to evaluate the risk of injury in a variety of aircraft and spacecraft systems [18-19]. The Brinkley model estimates the likelihood of injury using a spring/mass/damper lumped parameter representation of the body for each axis (x – chest to back direction, y – sideways direction, and z – vertical or spinal direction) of the occupant. The coefficients of these lumped parameters in the mathematical formulation are based on experiments conducted on volunteers from the U.S. Army and Navy. For more information on the development and use of the Brinkley model, see refs [16] and [18].

Seat pan acceleration time history pulses in all three directions are input into the Brinkley model. The output result from the Brinkley model is the beta value, which is an index taking into account responses from all three axes. The value of beta is given for three risk categories (low, medium and high), and a beta value greater than one in a particular category pushes the injury probability into the next higher category. Table 4 lists the beta values for all occupants for both tests.

Table 4 – Beta values from Brinkley Model

	<i>Beta Low</i>	<i>Beta Med.</i>	<i>Beta High</i>
Pilot	1.87	1.56	1.22
Co-pilot	1.78	1.49	1.17
Rear Passenger	1.24	1.01	0.81

The results shown in Table 4 reinforce the results seen from both the Eiband criteria and the lumbar load criteria. Both the pilot and co-pilot are at a high risk of injury (denoted by beta larger than one value in the “Beta High” column), while the rear passenger is at a medium risk of injury.

Finally, Head Injury Criteria (HIC) [20] values were evaluated for the three occupants. Table 5, shows the output HIC value. Note that HIC 36 was used and its limit for injury is 1,000. The HIC value is a unit-less number and the limit corresponds to a probability of head injury, as determined by the AIS Scale [21].

Table 5 – HIC Values

	<i>HIC</i>
Pilot	94
Co-pilot	110
Rear Passenger	103

All HIC values were generally around 100, and were much lower than the injury limit cutoff of 1000. Typically, high values of HIC result when the occupant’s head strikes an object. The low values indicate a low probably of head injury, which is consistent with inspections of the ATDs post-test, along with examination of the high speed video, which showed that a head strike for any of the occupants did not occur. The HIC was the only measurable injury criteria used where the injury probabilities were low, as all of the others examined gave a moderate to high probability of injury.

### Summary

A full-scale crash test of an MD-500 helicopter was conducted at NASA LaRC LandIR facility on March 10th, 2010. The crash test was a part of a larger test series in which one of the objectives was to validate a novel deployable energy absorbing concept on an actual airframe under realistic crash conditions. This report described the unmodified MD-500 test which served as a baseline for which to compare. Along with serving as a baseline, the test gave engineers valuable insight into the response of a small helicopter subject to impact loads. A third objective of the test was to provide validation data for a finite element simulation of an MD-500 helicopter.

The results indicated there was substantial airframe damage in the lower subfloor and keel beam. Accelerations were on the order of 51.3 g for the front of the airframe and 41.9 g for the rear of the airframe with a pulse width between 10 and 40 ms. The helicopter was instrumented with four onboard ATDs; three of which were used to measure conventional internal ATD acceleration and loads, while the fourth ATD was a specialized torso model measuring internal organ pressures.

The occupant response data was passed through a variety of injury criteria; most of which gave a moderate to severe risk of injury. The only criteria which gave a low probably of injury was the HIC. The conclusions drawn from the results of the injury criteria established that the occupants would have a moderate to high probably of injury from spinal compression loads as noted by the lumbar load criteria. However, both the Brinkley model and the Eiband criteria are whole body criteria and do not distinguish individual or specific location for injury, but

suggest that the probability of injury to an occupant is moderate to high.

Full-scale crash testing can further understanding of events seen during the impact process. It can also provide valuable data for the evaluation of injury and insights into vehicle dynamics for use in the future.

## References

- [1] O'Bryan, T. C., and Hewes, D. E., "Operational Features of the Langley Lunar Landing Research Facility," NASA TN D-3828, February 1967.
- [2] Jackson, K.E. et al. "A History of Full-Scale Aircraft and Rotorcraft Crash Testing and Simulator at NASA Langley Research Center." NASA TM 2004-178862. 2004.
- [3] Code of Federal Regulations. Federal Aviation Regulations for Aviation Maintenance Technicians FAR AMT, Part 27 Airworthiness Standard: Normal Category Rotorcraft, 27.562 Emergency Landing Dynamics.
- [4] Code of Federal Regulations. Federal Aviation Regulations for Aviation Maintenance Technicians FAR AMT, Part 29 Airworthiness Standard: Transport Category Rotorcraft, 29.562 Emergency Landing Dynamics.
- [5] Society of Automotive Engineers. "Performance Standard for Seats in Civil Rotorcraft, Transport Aircraft, and General Aviation." SAE AS8049a. July 1990.
- [6] Kellas S., "Deployable Rigid System for Crash Energy Management," US Patents 6,755,453, June 29, 2004, 6,976,729 December 20, 2005, and 7,040,658 May 9 2006.
- [7] Kellas S. and Jackson K. E., "Deployable System for Crash-Load Attenuation," Proceedings of the 63rd AHS Annual Forum, Virginia Beach, VA. May 1-3, 2007.
- [8] Kellas S. and Jackson K.E., "Multi-Terrain Vertical Drop Tests of A Composite Fuselage Section." Proceedings of the 64<sup>th</sup> Annual AHS Forum, Montreal, Canada. April 29-May 1, 2008.
- [9] Kellas, S., Jackson, K., and Littell, J., "Full Scale Crash Test of a MD 500 Helicopter with Deployable Energy Absorbers," Proceedings of the 66th AHS Annual Forum, Phoenix, AZ, May 11-13, 2010.
- [10] Annett, M. S., Polanco, M. A., "System-Integrated Finite Element Analysis of a Full-Scale Helicopter Crash Test with Deployable Energy Absorbers," Proceedings of the American Helicopter Society 66<sup>th</sup> Annual Forum, Phoenix, AZ, 11-13 May, 2010.
- [11] Gowdy, V. et al. "A Lumbar Spine Modification to the Hybrid III ATD for Aircraft Seat Tests". SAE 1999-01-1609. 1999.
- [12] Roberts, J., et al., "Computational and Experimental Models of the Human Torso for Non Penetrating Ballistic Impact." *Journal of Biomechanics*, Vol. 40, pp. 125-136, 2007.
- [13] Military Standard, MIL-STD-1290A (AV), Light Fixed- and Rotary-Wing Aircraft Crash Resistance, Department of Defense, Washington DC, 20301, 26 September 1988.
- [14] Littell, J.D. "Large Field Photogrammetry Techniques in Aircraft and Spacecraft Impact Testing" Proceedings from the Society of Experimental Mechanics Annual Conference. Indianapolis IN. June 7-10, 2010.
- [15] Eiband, A.M. "Human Tolerance to Rapidly Applied Accelerations: A summary of the Literature," NASA Memorandum 5-19-59E. 1959.
- [16] Society of Automotive Engineers. "Surface Vehicle Recommended Practice: Instrumentation for Impact Test-Part 1-Electronic Instrumentation". SAE J211-1, July 2007.
- [17] Brinkley, J.W., Specker, L.J., and Mosher, S.E., "Development of Acceleration Exposure Limits for Advanced Escape Systems." NATO AGARD Proceedings, AGARD-CP-472, February 1990.
- [18] Jackson K. E. et al. "Occupant Responses in a Full-Scale Crash Test of the Sikorsky ACAP Helicopter". *Journal of the American Helicopter Society*, Vol 49, No. 2. April 2004.

- [19] Lawrence C. et al. "The Use of Vehicle Acceleration Exposure Limit Model and a Finite Element Crash Test Dummy Model to Evaluate the Risk of Injuries During Orion Crew Module Landings". NASA TM 2008-215198. 2008.
- [20] U.S. Department of Transportation. "Federal Motor Vehicle Safety Part 571, Standard 208 – Occupant Crash Protection." [www.fmcsa.dot.gov](http://www.fmcsa.dot.gov). Accessed 11-12-10.
- [21] States, J.D. "The Abbreviated and the Comprehensive Research Injury Scales". SAE 690810. 1969.